# *Fire resistance of square double-skin concrete-filled steel tubular columns and concrete-filled double steel tubular columns*

Engineering Structures 319 (2024) 118882

Contents lists available at ScienceDirect

Engineering Structures

journal homepage: www.elsevier.com/locate/engstruct

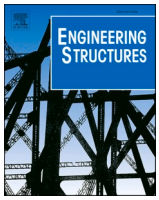

# Fire resistance of square double-skin concrete-filled steel tubular columns and concrete-filled double steel tubular columns

Hongjie Zhu [a], Mizan Ahmed [b], Chenliu Li [a], Xiao Kong [a], Shicai Chen [a,*], Qingtian Yang [c], Habibah Ghazali [d], Qing Quan Liang [d,*,1]

[a] Department of Civil Engineering, Beijing University of Technology, Beijing 100000, PR China
[b] Centre for Infrastructure Monitoring and Protection, School of Civil and Mechanical Engineering, Curtin University, Kent Street, Bentley, WA 6102, Australia
[c] Beijing Beiran Industrial Group Co. Ltd, Beijing 100000, PR China
[d] College of Sport, Health, and Engineering, Victoria University, PO Box 14428, Melbourne, VIC 8001, Australia

ARTICLE INFO

*Keywords:*
Concrete-filled steel tube
Double-skin
Double steel tubes
Fire resistance
Finite element simulation

ABSTRACT

Square double-skin concrete-filled steel tubular (DSCFST) columns and concrete-filled double steel (CFDST) columns possess excellent load-carrying capacity and ductility. However, there has been limited research on the responses of DSCFST and square CFDST columns exposed to fire. This paper presents a series of tests on such columns loaded concentrically to determine the effects of the steel tube thickness, the strength of materials, load ratio, and boundary conditions on their fire resistance. Additionally, finite element (FE) models are established using ABAQUS, in which the concrete's transient creep strain is considered through the development of the user-subroutine UEXPAN. A parametric study is undertaken by simulating 156 FE models to further study the behavior of DSCFST and CFDST columns under fire exposure. The fire test and numerical results suggest that both the load ratio and strengths of the internal tube and concrete core play significant roles in determining the fire resistance of DSCFST and CFDST columns. The developed FE models are demonstrated to capture well the fire behavior of loaded DSCFST and CFDST columns. The proposed design model predicts the ultimate loads of DSCFST columns with good accuracy; therefore, it can be employed in the practical design of DSCFST columns.

## 1. Introduction

Concrete-filled steel tubular (CFST) columns have been widely utilized to construct high-rise superstructures owing to their high ductility, load-carrying capacities, durability, and dynamic performance. While CFST columns with a circular section provide remarkable confining pressures to the concrete core, the ease of connections to the beams offered by the square section makes them an ideal choice for faster construction of composite structures. The structural performance of square CFST square columns subjected to various loading conditions has been extensively studied [1–5]. The failure modes associated with square CFST short columns were found to be the local buckling of the steel plate and concrete crushing. Furthermore, high-strength concrete (HSC) is widely employed in composite columns to increase their load-carrying capacities or reduce their cross-sectional sizes. However, filling composite columns with HSC leads to a decrease in their ductility due to the brittle behavior of HSC. To improve the structural behavior of CFST columns, square double-skin CFST (DSCFST) columns, and concrete-filled double steel tubular (CFDST) columns have been developed as illustrated in Fig. 1. The weight of a DSCFST column is lighter than that of a CFST column with the same size. The internal circular steel tube in a CFDST column provides confining stresses to the concrete core, thereby improving the structural behavior of the column.

Extensive research work has been conducted on square DSCFST and CFDST columns under axial and eccentric loading at room temperature [5–15]. Experimental results demonstrate that the ductility and strength of square CFDST columns are significantly higher than those of square CFST columns. The behavior of stocky DSCFST and CFDST columns are influenced by the strength of materials. However, slender columns primarily fail by the overall column buckling and thus the

strength of materials has less significance on their mechanical performance. However, materials may degrade when they are exposed to extreme conditions [16–18], and the research into the fire performance of DSCFST columns and CFDST columns has been very limited. Lu et al.

* Corresponding authors.
*E-mail addresses:* shicaichen@163.com (S. Chen), Qing.Liang@vu.edu.au (Q.Q. Liang).
[1] https://orcid.org/0000–0003-0333–2265

https://doi.org/10.1016/j.engstruct.2024.118882
Received 2 June 2024; Received in revised form 3 August 2024; Accepted 25 August 2024
Available online 31 August 2024

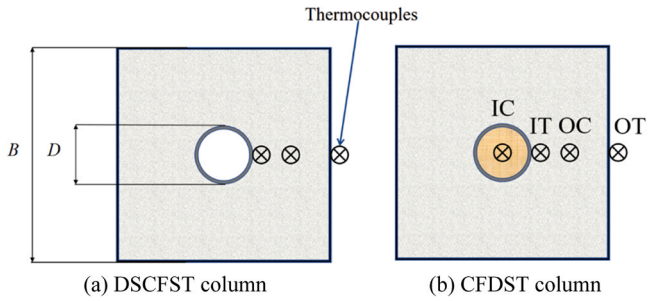


**Fig. 1.** Cross-sections of square columns.

[19] examined the fire resistance of DSCFST slender columns incorporating self-compacting concrete. The tested columns were loaded either concentrically or eccentrically and the effects of the different cross-sections of DSCFST columns were investigated. It was reported that the hollow ratio of the columns significantly affects the fire performance of DSCFST slender columns. Liu et al. [20] studied the responses of circular DSCFST columns under various fire durations. It was found that the concrete strength has an insignificant effect on the residual strength of the DSCFST columns after fire. Liu et al. [21] tested circular DSCFST stocky columns under fire to examine the effects of fire duration, the strength of materials, axial load ratio, and hollow ratio of the columns. It was found that the fire resistance of the columns is significantly affected by the hollow ratio of the columns.

Romero et al. [22] carried out fire tests on circular DSCFST and CFDST columns. It was concluded that if the inner tube is very thin, the improvement of the fire resistance is minimal compared to CFST columns. Camargo et al. [23] investigated the influences of material strength, load ratio, boundary conditions, and slenderness ratio on the fire behavior of DSCFST and CFDST slender columns of a circular section. It was reported that the loading ratio had significant effects but the material strength and thermal restraint had insignificant effects on the resistance of such columns to fire loading. Zhu et al. [24] investigated the fire resistance of circular DSCFST and CFDST columns and proposed a design model for fire resistance. It was found that the fire resistance time of CFDST columns is higher than that of DSCFST columns because the inner tube is filled with concrete. Lope et al. [25,26] studied the influence of concrete strength, column slenderness, and restraint stiffness on the fire performance of DSCFST and CFDST columns. It is concluded that the effect of the concrete strength is insignificant and a new design model is required for CFDST columns. Abdelrahman et al. [27] formulated numerical models to study the heat transfer of various cross-sections of DSCFST columns. The accuracy of the available models for the thermal modeling of the composite section including the thermal properties of various materials and models for simulating thermal contact of the interactions of steel and concrete was examined. The effects of various materials on the fire performance of DSCFST columns were analyzed. It was concluded that filling normal strength concrete in the outer tube and higher strength concrete in the inner tube can improve the fire resistance of the columns.

Limited research work has been undertaken to examine the responses and working mechanism of square CFDST columns exposed to fire and to date, no design model has been developed. To overcome the limitations, in this paper, the fire test program and measured results are described on square DSCFST and CFDST columns loaded concentrically. The effects of material strength, load ratio, boundary condition, and steel tube thickness on the resistance of such columns to fire are examined. Finite element simulation models are also developed, and their accuracy is confirmed by experiments. A detailed parametric investigation is carried out to ascertain the influences of various parameters on the fire resistance of such columns. The load distributions in DSCFST and CFDST columns exposed to fire are analyzed using the FE model. A design model for concentrically loaded square CFDST slender columns under fire exposure is formulated and validated.

## 2. Fire test program

### 2.1. Details of the specimens

Nine specimens including eight CFDST columns and one DSCFST column were tested under fire. The details of the column specimens are given in Table 1. Specimen F-1 is a DSCFST column and specimens F-2 to F-9 are CFDST columns with an inner tube filled with concrete. The width of the external tubes and the diameter of the internal tubes were identical for all specimens; however, the tube thickness was changed to study its effects on fire resistance. Two different width-to-thickness

($B/t$) ratios of the outer tubes and diameter-to-thickness ($D/t$) ratios of the inner tubes were designed. All specimens had a length ($L$) of 1300 mm. However, during the tests, the column length exposed to fire was only 700 mm. The relative slenderness ratio ($\bar{\lambda}$) varied from 0.36 to 0.41, which was determined by the following formula based on EN 1993 part 1–1 [28].

$$\bar{\lambda} = \sqrt{\frac{N_{pl}}{N_{cr}}} = \sqrt{\frac{A_{os}f_{os} + A_{oc}f_{oc} + A_{is}f_{is} + A_{ic}f_{ic}}{\pi^2\left(E_{os}I_{os} + E_{is}I_{is} + 0.6E_{oc}I_{oc} + 0.6E_{ic}I_{ic}\right)/l^2}} \quad (1)$$

where $A$ stands for the cross-sectional area; $I_{is}$ and $I_{os}$ define the moment of inertia of internal and external steel tubes, respectively; $E_{is}$ and $E_{os}$ are elastic moduli of inner and outer steel tubes, respectively; $E_{oc}$ and $E_{ic}$ are the secant modulus of sandwiched concrete and core concrete,

**Table 1**
Details of DSCFST and CFDST column specimens.

| Specimen | $B$ (mm) | $f_{s,os}$ (MPa) | $t_o$ (mm) | $f_{c,oc}$ (MPa) | $D$ (mm) | $f_{s,is}$ (MPa) | $t_i$ (mm) | $f_{c,ic}$ (MPa) | $n$ | $\bar{\lambda}$ | $P_r$ (kN) | B.C | Time (min) |
|---|---|---|---|---|---|---|---|---|---|---|---|---|---|
| F−1 | 200 | 330 | 4 | 54 | 108 | 604 | 6 | - | 0.45 | 0.36 | 1342 | P-F | 92 |
| F−2 | 200 | 330 | 3 | 54 | 108 | 330 | 8 | 54 | 0.45 | 0.40 | 1433 | P-F | 111 |
| F−3 | 200 | 330 | 4 | 54 | 108 | 330 | 6 | 54 | 0.45 | 0.37 | 1212 | P-F | 100 |
| F−4 | 200 | 330 | 4 | 54 | 108 | 604 | 6 | 54 | 0.4 | 0.40 | 1363 | P-P | 98 |
| F−5 | 200 | 330 | 4 | 54 | 108 | 604 | 6 | 54 | 0.45 | 0.40 | 1533 | P-F | 120 |
| F−6 | 200 | 330 | 4 | 54 | 108 | 604 | 6 | 64 | 0.45 | 0.41 | 1538 | P-F | 131 |
| F−7 | 200 | 330 | 4 | 64 | 108 | 604 | 6 | 54 | 0.45 | 0.41 | 1796 | P-F | 94 |
| F−8 | 200 | 330 | 4 | 54 | 108 | 604 | 6 | 54 | 0.45 | 0.40 | 1534 | P-P | 91 |
| F−9 | 200 | 330 | 4 | 54 | 108 | 604 | 6 | 54 | 0.55 | 0.40 | 1874 | P-F | 58 |
| Y−4 [24] | 219 | 330 | 4 | 54 | 108 | 604 | 6 | 54 | 0.4 | 0.34 | 1318 | P-P | 137 |

Note: $B$ and $t_o$ stand for the width and thickness of the outer steel tube, respectively; $D$ and $t_i$ are the diameter and thickness of the inner steel tube, respectively; $f_{s,}$ and $f_{c,}$ denote steel yield and concrete strength, respectively, and subscripts $os$, $oc$, $is$, and $ic$ represent the outer steel tube, sandwiched concrete, inner steel tube, and core concrete, respectively; $\bar{\lambda}$is the relative slenderness ratio; $n$ represents the load ratio; $P_r$ represents the applied load; B.C means the boundary condition; P-F and P-P are pinned-fixed and pinned-pined boundary conditions, respectively.

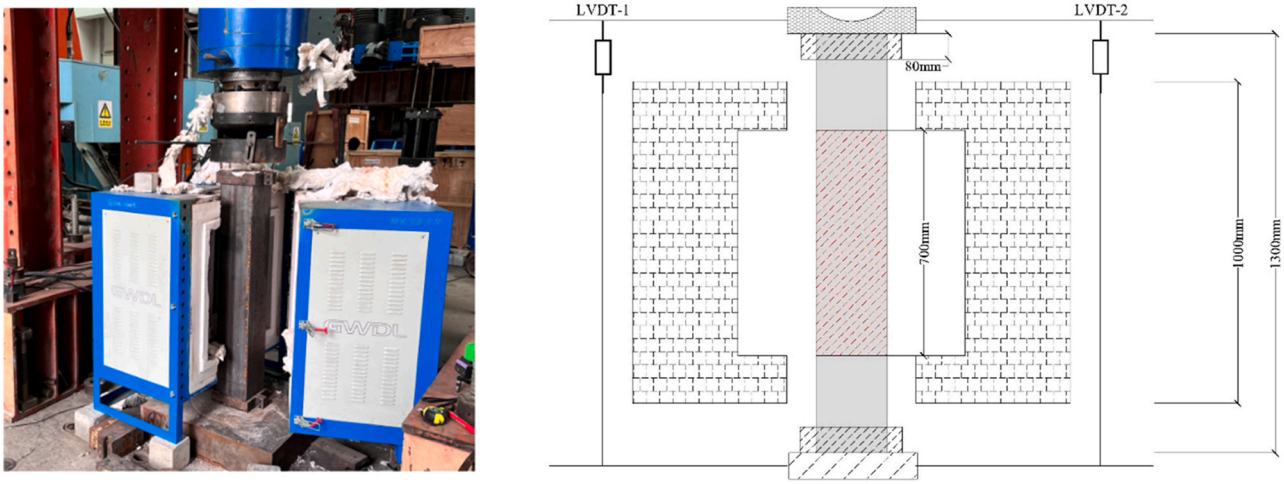


(a) Outside view (b) Schematic view

**Fig. 2.** Test setup.

respectively.

Three load ratios (0.4, 0.45, and 0.55) and two boundary conditions (pinned-pinned and pinned-fixed) were considered in the experiment. Two different concrete strengths were used to investigate the effects of concrete strength on the fire resistance of column specimens.

### 2.2. Properties of materials

The compressive strengths of concrete were determined by compression tests on concrete cubes according to Chinese Standard GB/T 50081–2002 [29]. After 28 days of curing, the mean compressive strengths were measured as 54 and 64 MPa, respectively. The outer steel tube was made of Q235 structural steel, while two categories of structural steel Q235 and Q460 were adopted for the internal steel tube. A static tensile test was undertaken to obtain the mechanical properties of steel according to Chinese code [30]. The measured average yield stresses of the Q460 and Q235 steels were 604 and 330 MPa, respectively.

### 2.3. Test procedure

The fire tests were conducted at the Beijing University of Technology, China. The test setup of the column specimen is illustrated in Fig. 2. Two loading stages were adopted for the test. The column specimen was first loaded concentrically via a loading frame with a capacity of 3000 kN. A displacement method was used in the loading stage, and the rate was selected to be 2 mm/min. Once the designed load was reached, it was held constant. An electric furnace was then employed to heat the specimen to simulate the real fire condition. The furnace was configured to heat the specimen following the ISO-834 standard fire curve [31]. Two ventilation holes having a diameter of 20 mm were drilled at 50 mm from the two ends of the specimen. To monitor the instantaneous temperature, thermocouples were positioned at the column mid-height across its cross-section, as depicted in Fig. 1. Two displacement gauges were affixed to each side of the loading plate to track real-time displacement. The fire test was stopped when the axial displacement reached 13 mm, or its axial displacement velocity exceeded 3.9 mm/min. The critical time representing the fire resistance of each specimen taken when the axial displacement reached 0.01 $L$ or the velocity reached 0.003 $L$/min is shown in Table 1.

## 3. Test results

### 3.1. Failure characteristics

The global failure modes of the column specimens are shown in Fig. 3. Generally, specimens failed by the global buckling associated with local buckling. The localized buckling of the steel tube occurred in the middle region of the column. For the columns with pinned-pinned boundary conditions (F-4 and F-8), the lateral deformation was greater than that of their fixed-fixed counterparts.

The external steel tube of F-9 was removed to examine the failure pattern of the concrete, as shown in Fig. 4(a). It was observed that the sandwiched concrete was crushed at the position where local buckling occurred. Additionally, Fig. 4(b) illustrates that although the specimen buckled globally, the internal steel tube did not undergo local buckling and the concrete core did not crush.

### 3.2. Distributions of temperatures

The typical distributions of the temperatures of the DSCFST column (F-1) and CFDST column specimens (F-3, and F-5) are plotted in Fig. 5. It can be observed from Fig. 5 that the furnace temperature-time curves are similar for the fire tests of three specimens. However, the furnace temperature is lower than the temperature calculated by the standard ISO-834 fire curve since the maximum power of the electric furnace is limited. Such a phenomenon is common if an electrical furnace is used, as reported by Liu et al. [32]. In the initial heating stage, the temperature of the external steel tube increased rapidly as it was directly exposed to fire. Accordingly, it was significantly higher than the temperatures of other components in the specimen. For example, in

the case of specimen F-5, when it failed, the temperature of its external steel tube exceeded that of the sandwiched concrete, internal steel tube, and concrete core by approximately 400, 500, and 700°C, respectively. The increase in the temperatures of the internal steel tube and concrete components exhibited a delay when reaching temperatures between 100 and 200°. This delay was due to the water evaporating within the concrete. Moreover, compared to specimen F-1, the temperatures of the internal steel tubes in specimens F-3, and F-5 increased slowly. For instance, at the 80-min exposure time, the temperatures of the internal steel tube of specimens F-1, F-3, and F-5 were 410°C, 366°C, and 325°C, respectively. Again, such a phenomenon was caused by the water evaporation from the core concrete.

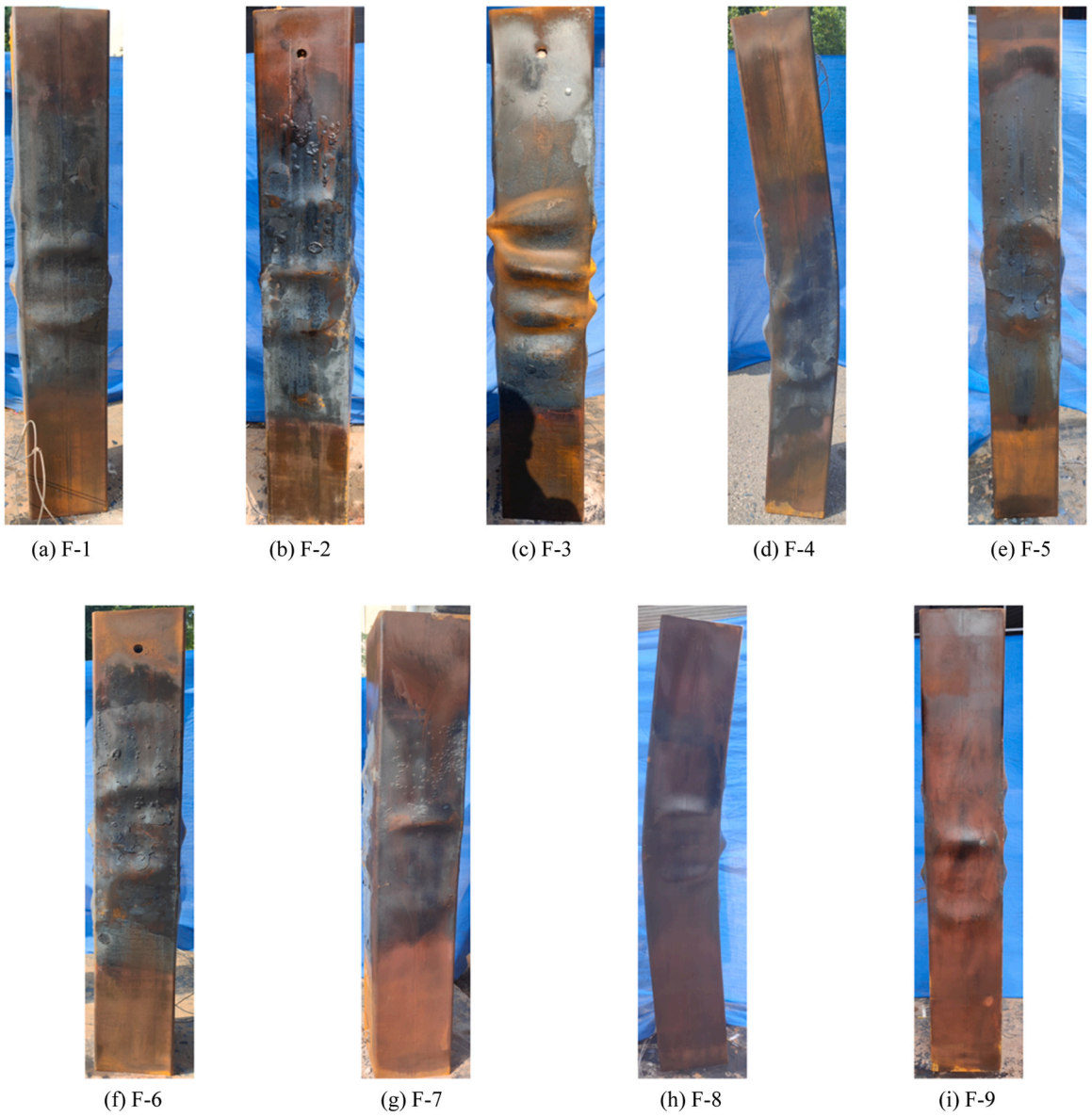


**Fig. 3.** Failure modes of columns.

### 3.3. Axial displacement and velocity curves

The axial shortening vs time relationships of tested columns in the second test procedure are presented in Fig. 6, which excludes the deformation caused by the applied load. In general, the behavior of a specimen can be described in three stages. In the first stage, during the unchanged portion of the axial displacement curve, the external steel section was heated directly. It expanded thermally and became the main part that sustained the applied load. In the second stage, the external steel tube yielded and degraded owing to high temperatures. Consequently, the axial displacement curve showed a steady increase, and the sustained load was transferred to both the internal tube and the filled concrete. In the third stage, the inner tube and sandwiched concrete degraded due to the combined effects of high temperatures and plastic loading. As a result, the core concrete primarily supported the applied load. Therefore, the rise in the axial displacement accelerated and eventually, the temperature within the cross-section became so high that the specimen could not sustain the applied load anymore. A sharp increase in the axial displacement curve observed in Fig. 6 indicates that the specimen failed at that moment. Fig. 6 shows that the axial displacement of specimens F-1, F-2, F-5, F-6, F-7, and F-8 started to increase when the heating time was approximately 20 min. However, the exposure times for specimens F-3, F-4, and F-9 were approximately 40, 40, and 15 min, respectively. The differences in displacements can be primarily attributed to the differences in the applied load to these specimens. Furthermore, the strength of specimen F-3 at room temperature was relatively lower because the inner steel tube had a yield strength of 330 MPa only. Under the same load ratio, the load applied to specimen F-3 was less. Accordingly, the external steel tube yielded later than other specimens, delaying the increase in the axial displacement.

### 3.4. Effects of material strengths

Fig. 7(a) and (b) illustrate the effect of the strengths of core and sandwiched concrete on the fire resistance of DCFST and CFDST columns. The sandwiched concrete in specimens F5, and F6, had the same strength but the inner tube of F6 had higher yield strength than F5. As shown in Fig. 7(a), CFDST columns have higher fire resistance than DSCFST columns. Compared with the DSCFST specimen (F-1), the fire resistance of CFDST specimens (F-5 and F-6) increased by 30 % and

(a) Failure mode of the sandwiched concrete

(b) Interaction between core concrete and steel tube

**Fig. 4.** Failure state of the specimen F-9.

42 %, respectively. Fire resistance is further extended when higher compressive strength concrete is used for the core. For instance, changing the compressive strength of the core concrete.

from 54 MPa (F-5) to 64 MPa (F-6) leads to a 9 % rise in the fire resistance time. This is because the inner steel tube confined the core concrete. However, as illustrated in Fig. 7(b), when the load ratio was constant, the column (F7) filled with higher-strength concrete exhibited a shorter fire resistance time than the specimen (F5) with lower sandwiched concrete strength. The fire resistance of specimen F-7 (64 MPa) was 21 % shorter than that of specimen F-5 (54 MPa). The external square steel tube exposed to fire underwent local buckling so that it could not confine the sandwiched concrete. Therefore, it is recommended to fill higher-strength concrete in the inner tube and lower-strength concrete in the sandwiched section. Furthermore, using an inner tube having a higher yield strength increases the fire resistance of CFDST columns as shown in Fig. 7(c). As the yield strength increased from 330 MPa (F-5) to 604 MPa (F-3), there was a 16 % increase in the fire resistance time for specimen F5. Thus, using an inner steel tube with a higher yield strength or filling it with high-strength concrete can improve the fire performance of the CFDST column.

### 3.5. Effects of the thicknesses of the steel

Fig. 8 compares the impact of varying the thicknesses of steel tubes and the shape effects of CFDST columns on their fire resistance. Compared with specimen F-2 ($t_o$= 3 mm and $t_i$= 8 mm), the fire resistance time of specimen F-3 ($t_o$= 4 mm and $t_i$= 6 mm) was reduced by 9 %. This hints that the fire resistance of CFDST columns can be improved by increasing the thickness of steel tubes. It should be pointed out that the external tube was exposed to high temperatures directly so that its properties degraded sharply in a short time. However, when a thicker inner steel tube was used, a greater portion of the internal steel profile was under thermal protection, thereby enabling the full potential of steel reinforcement to enhance the load-bearing capacity.

To understand the shape effects, the fire resistance time of a CFDST column (specimen F4) is compared to that of a circular CFDST column (specimen Y5) reported by the authors previously [24]. The details of column specimen Y5 are also listed in Table 1. As shown in Fig. 8(b), if the material usage is similar, a circular column performs better than its square counterpart in a fire condition. When the area is fixed, a square section has a higher perimeter value than a circular section. This means that the directly heated surface area of a square section is larger, resulting in the temperature within the square column rising faster. Moreover, in a fire condition, a square column is heated non-uniformly, which may cause thermal stress within the column. Thus, a square column reaches its fire resistance earlier than a circular column.

### 3.6. Effects of the loading ratio and boundary conditions

The fire responses of specimens F-5 ($n$ = 0.45) and F-9 (n = 0.55) with different load ratios are

compared. As depicted in Fig. 9(a), the load ratio significantly diminishes the fire resistance of the columns. The fire resistance time is reduced by 51 % when the loading ratio is increased from 0.45 to 0.55. This phenomenon is consistent with the other test results of filled composite columns in the fire as discussed by Wang et al. [33].

Furthermore, Fig. 9(b) indicates that the boundary condition affects the fire resistance of the column significantly. When the boundary condition is changed from pinned-pinned condition (specimen F-8) to pinned-fixed condition (specimen F-5), the fire resistance increases by 32 %. This is because the variation in the boundary condition alters the Euler buckling load [34,35], and a similar conclusion was reported in previous studies [23,36,37].

## 4. Finite element analysis

### 4.1. FE modeling

An FE model was established by the sequentially coupled method to determine the temperature field and stress distributions of CFDST columns under fire exposure. A heat-transfer analysis was performed first to obtain the temperature evolution of the FE model. Then, the temperature field was inputted into the stress analysis to simulate the mechanical behavior of the column under fire exposure. The tested column was modeled, and the approximate mesh size of steel tubes and concrete

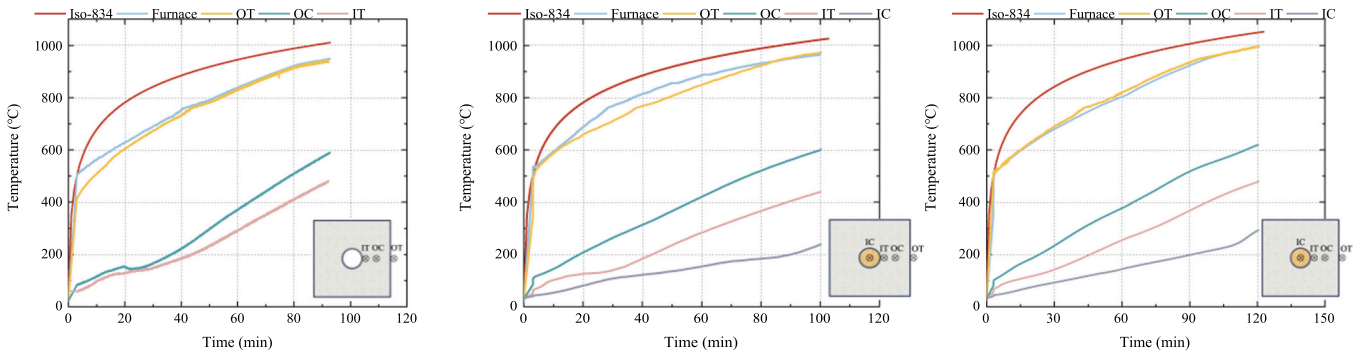


(a) F-1 (b) F-3 (c) F-5

**Fig. 5.** Temperature distributions of tested specimens.

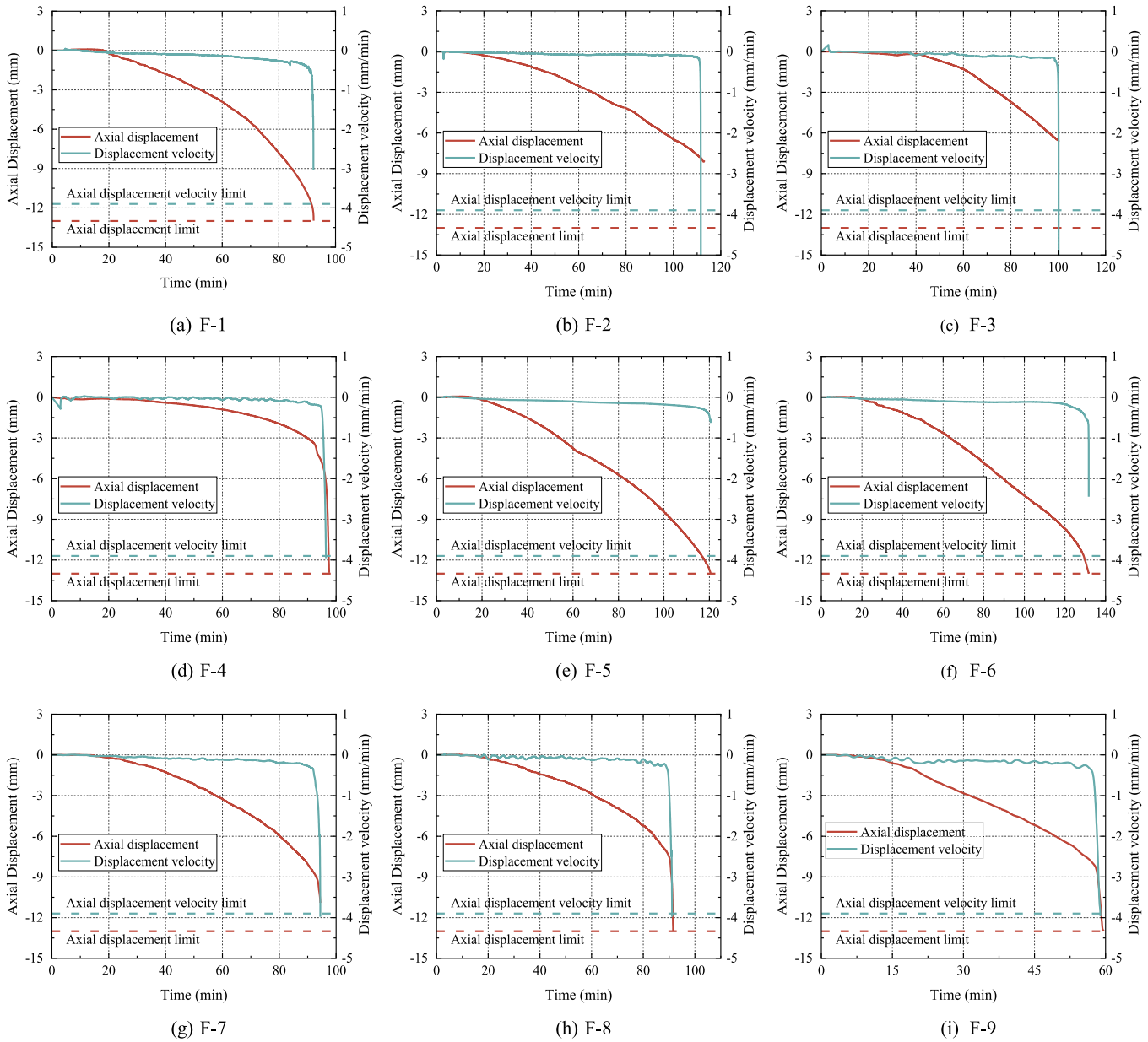


**Fig. 6.** Axial displacement-time curves.

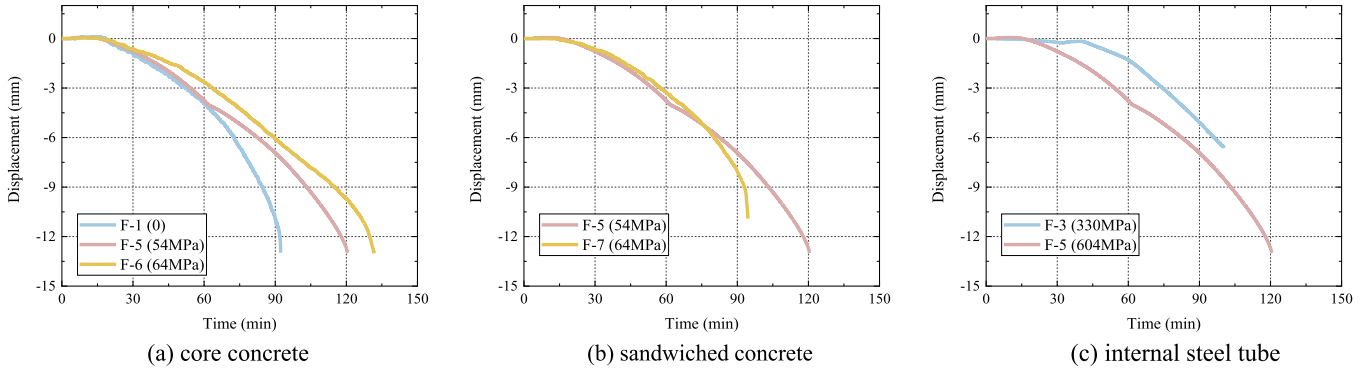


**Fig. 7.** Influences of material strengths on the fire resistance of CFDST columns.

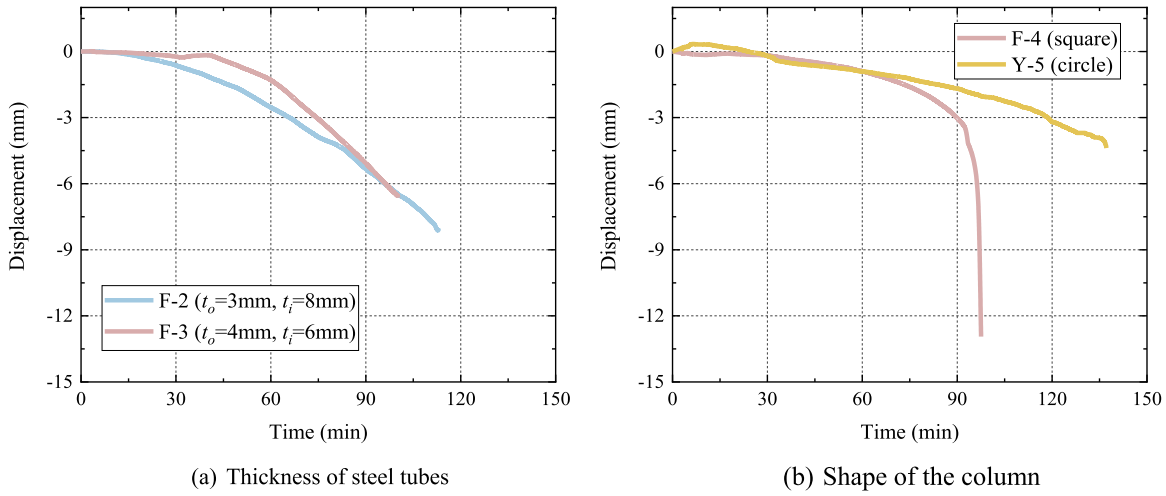


**Fig. 8.** Significance of the thickness and shapes of the steel tube on the fire resistance of CFDST columns.

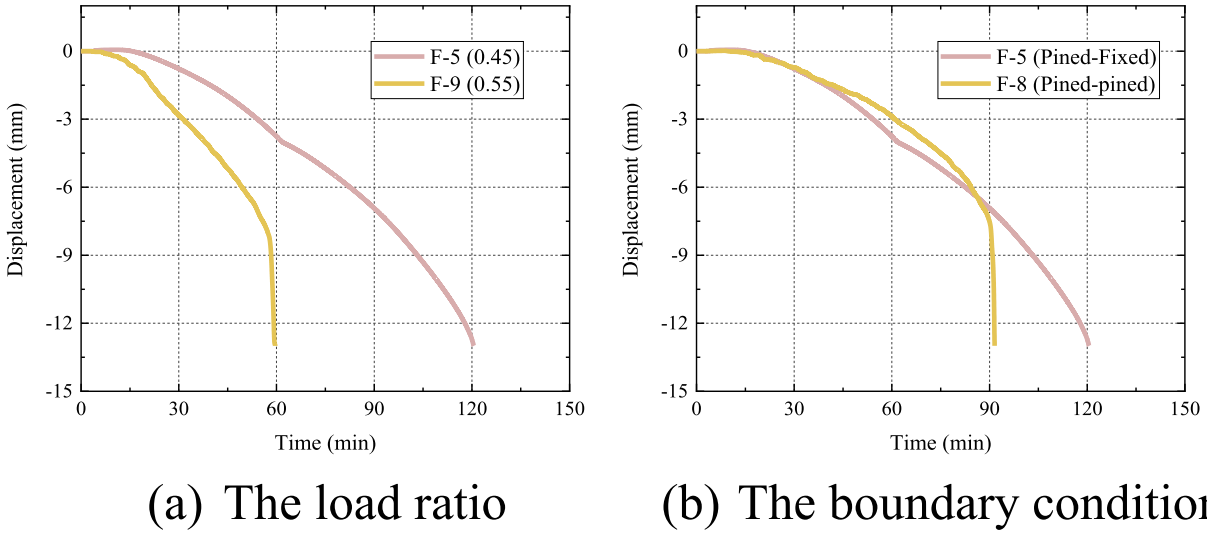


**Fig. 9.** Significance of the loading ratio and boundary conditions on the fire resistance of CFDST columns.

components was 20 mm.

In the development of the heat transfer analysis, the thermal properties of materials, including thermal expansion, specific heat as well as thermal conductivity, were selected based on the recommendation given by Espinos et al. [38]. The measured temperature-time curves were applied to the surface directly exposed to fire. A film coefficient of 25 ($Wm^2$/K) and emissivity of 0.7 were adopted to simulate the convection and radiation mechanisms according to EN 1991–1-2 [39]. Additionally, the steel-concrete gap conductance affects the accuracy of the heat transfer analysis [38]. In the present study, a constant value of 200 $W/m^2$ was used to model this behavior.

In the stress analysis step, a constant axial load was applied to the top of the column, and the calculated temperature distribution of each node in the FE model was imported to determine the response of the column under fire exposure. The constitutive models of the materials proposed by Lie [40] were adopted. Concrete-damaged plasticity was employed to model concrete material. The tensile strength of the concrete suggested by Han et al. [41] was employed and its evolution was represented by the fracture energy which was taken as 240 N/m [41]. Existing studies [42–45] show that the load-induced strain distinctly affects the behavior of a concrete member exposed to fire. It depends on the stress state and temperature increment, but it was not incorporated in the constitutive model provided by Lie [40]. In this study, the model developed by Pearce [46] was employed to calculate the load-induced strain components:

$$\dot{\varepsilon}_{ij}^{list} = \frac{\beta}{f_{c0}}\left[(1+\mu T)\bar{\sigma_{ij}} - \mu T\bar{\sigma_{kk}}\delta_{ij}\right]\dot{T} \tag{2}$$

$$\beta = 0.01\begin{cases} 0.0008\overline{T} + 0.001 & 0 \le \overline{T} \le 4.5 \\ 0.014(\overline{T} - 4.5) + 0.0008\overline{T} + 0.001 & \overline{T} > 4.5 \end{cases} \tag{3}$$

$$\overline{T} = \frac{T - 20}{100} \tag{4}$$

in which $\dot{\varepsilon}_{ij}^{list}$ is the load-induced strain tensor, $\bar{\sigma_{ij}}$ is the compressive stress tensor in the current incremental step, $\bar{\sigma_{kk}}$ is the principle compressive stress components, $\delta_{ij}$ is the Kronecker delta, $f_{c0}$ is the compressive strength at room temperature, and $\mu T$ stands for the Poisson's ratio at elevated temperatures which can be calculated according to Gernay et al. [47]. The model was implemented through the user-subroutine UEXPAN.

A hard contact mechanism was utilized to model the interaction between the concrete and steel in the normal direction. The interaction in the tangent direction was simulated by a Coulomb friction model with a friction coefficient of 0.6. Espinos et al. [38] reported that initial

**Table 2**
Comparison between the test data and prediction.

| Column | $t_{FE}$ (min) | $t_{experiment}$ (min) | $t_{FE/experiment}$ |
|---|---|---|---|
| F−1 | 83 | 92 | 0.90 |
| F−2 | 127 | 111 | 1.14 |
| F−3 | 116 | 100 | 1.16 |
| F−4 | 82 | 98 | 0.84 |
| F−5 | 102 | 120 | 0.85 |
| F−6 | 116 | 131 | 0.89 |
| F−7 | 95 | 94 | 1.01 |
| F−8 | 73 | 91 | 0.80 |
| F−9 | 68 | 58 | 1.17 |
| R−1 [49] | 18 | 21 | 0.86 |
| SS1[19] | 101 | 115 | 0.88 |
| T5-DT-PC-K1 −50 [25] | 83 | 95 | 0.87 |
| Mean | | | 0.94 |
| Standard deviation | | | 0.14 |
| Coefficient of Variation | | | 0.14 |

imperfection has an impressive impact on the FE analysis of the column under axial loading. A small value of the initial imperfection yields a longer fire resistance time, while a large value reduces it. Hence, following Espinos et al. [38] and Zhu et al. [24], a value of $L/1000$ was used in the FE modeling, in which $L$ is the total column length.

In the current numerical analysis, when the analysis did not converge, a minimum incremental step of 0.01 was adopted. To avoid the convergence problem caused by material degradation due to high temperature, the automatic static stabilization method was employed [48], which adopts a damping factor of $1e^{-6}$.

### 4.2. Validation of the FE model

Experimental results on square CFDST columns obtained from the present study and those given by Han et al. [49], Lu et al. [19], and Lopes and Rodrigues [25] are used for the validation of the developed FE model. Table 2 compares the predicted and measured fire resistance times of CFDST columns. It appears from Table 2 that the mean value of the predicted to the measured fire resistance times is 0.94. The simulated and experimentally measured temperature-time and displacement-time curves for these columns are given in Figs. 10 and 11, respectively. It is shown that the simulations by the FE model are generally in good agreement with test data. As demonstrated in Fig. 12, the failure modes of columns F-1, F-4, and F-5 are well captured by the FE model.

## 5. Parametric study

The developed FE model was further employed to carry out a parameter study. The FE model was designed to be heated under the standard ISO-834 fire. The reference column was specified as follows: $B = 200$ mm, $t_o = 4$ mm, $D = 100$ mm, $t_i = 4$ mm, $f_{s,os} = f_{s,is} = 200$ MPa, $f_{c,oc} = f_{c,ic} = 40$ MPa, and $n = 0.4$. According to Zhu et al. [24], the fire performance of circular CFDST columns is affected by several factors, including material strength, cross-sectional properties, column slenderness and load ratio. Hence, in the present study, a total of 156 FE models were developed to ascertain the effects of 13 different influencing parameters on the fire performance of CFDST columns. The study covered different ranges of parameters: $B$= 200–500 mm, $D$= 40–140 mm, $t_o$= 2–20 mm, $t_i$= 2–20 mm, $D/B$= 0.3–0.7, and $t_i/t_o$= 0.8–1.2, $f'_{c,oc}$= 20–120 MPa, $f'_{c,ic}$= 0–120 MPa, $f_{s,os}$= 200–700 MPa, $f_{s,is}$= 200–700 MPa, $n$ = 0.1–0.55, and $\bar{\lambda}$= 0.2–1.0, as shown in Table 3. The selection of the material strength covered the normal and high-strength materials, and the dimensions of the FE columns were designed according to Table B.2 of EN 10210–2 [50]. For convenience, the column with a slenderness ratio ($\bar{\lambda}$) of 0.8 and 0.4 is defined as a slender and a stocky column, respectively. The ultimate load of the columns was computed by using the model of Ahmed et al. [51].

### 5.1. Influences of cross-sectional properties

The influences of the thickness and diameter of the internal tube, the thickness and diameter of the external tube, the $D/B$ ratio, $t_i/t_o$ ratio, and the shape of the columns on the fire resistance of CFDST columns were examined. It can be observed from Fig. 13 that the fire performance of the stocky column is remarkably higher than that of the slender column. In addition, the diameter of.

the internal tube has a minor effect on the fire resistance of stocky columns. However, enlarging the diameter of the inner tube increases the fire resistance of slender columns. When the inner tube diameter is increased to 140 mm, the fire resistance of the column rises by 37 %. Increasing the diameter increases the cross-sectional area of the core concrete, thereby improving the resistance of CFDST columns to fire loading.

It can be observed from Fig. 13 (b) that the fire resistance time of the CFDST column increases with rising the thickness of the internal tube, regardless of the column slenderness ratio. Such a phenomenon can be attributed to the confinement effect on the core concrete as well as the additional steel to support carrying the load at elevated temperatures. However, the rate of increase in the fire resistance time of stocky columns caused by concrete confinement is remarkably higher than that of the slender columns. Hence, a design strategy for CFDST columns is increasing the thickness of the internal steel tube, which complies with the observations from Romero et al. [22] and Zhu et al. [24].

Fig. 13 (c) and (d) show the effects of the dimension ($B$) and thickness ($t_o$) of the outer steel tube on the fire resistance of CFDST columns. As expected, as the $B$ enlarges, the fire resistance of the CFDST column increases with increasing the cross-sectional area of the concrete. As

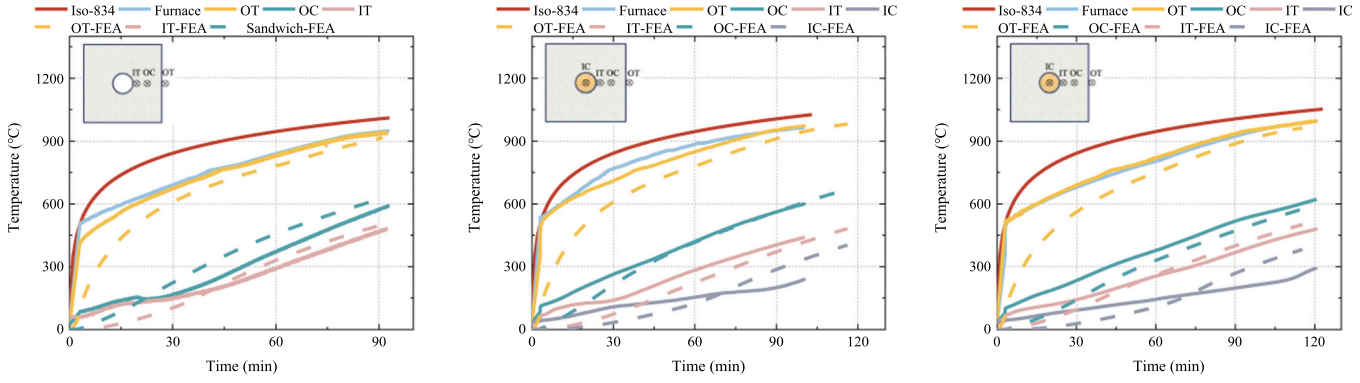


(a) F-1 (b) F-3 (c) F-5

**Fig. 10.** Verification of temperature-time curves.

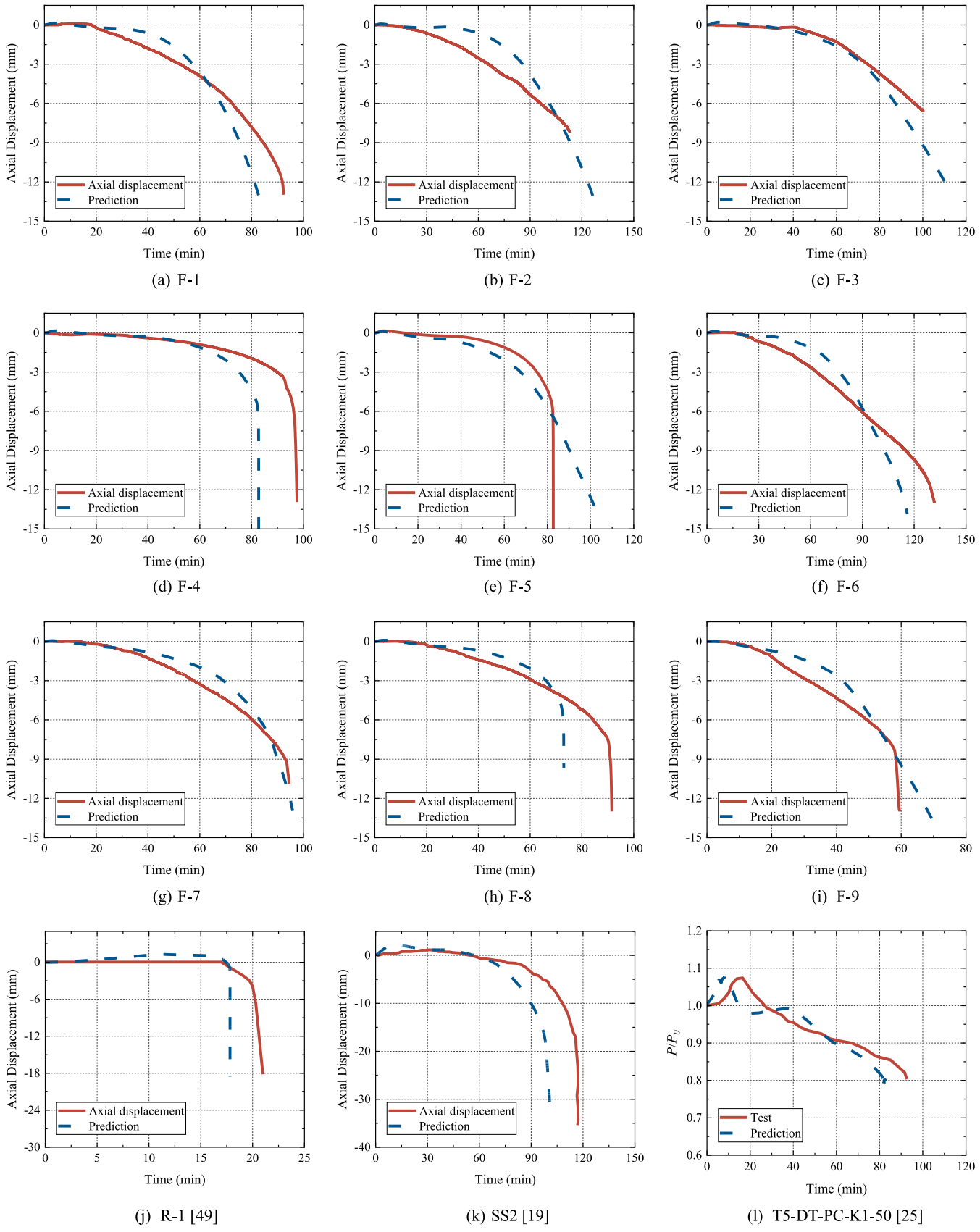


**Fig. 11.** Verification of displacement-time curves.

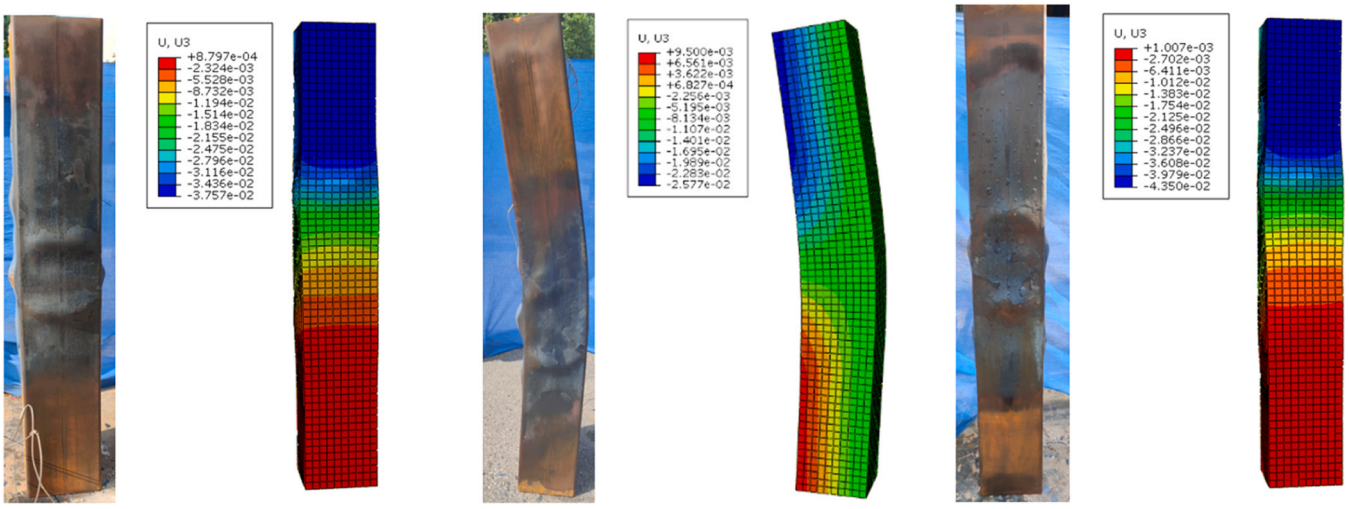


(a) F-1 (b) F-4 (c) F-5

**Fig. 12.** Comparison of failure modes.

**Table 3**
Details of the analyzed parameters.

| Parameters | | Default value |
|---|---|---|
| $t_i/t_e$ | 0.8, 0.9, 1.0, 1.1, and 1.2 | 1.0 |
| $D/B$ | 0.3, 0.4, 0.5, 0.6, and 0.7 | 0.5 |
| $B$ (mm) | 200, 250, 300, 350, 400, 450, and 500 | 200 |
| $D$ (mm) | 40, 60, 80, 100, 120, and 140 | 100 |
| $f_{c,oc}$ (MPa) | 20, 40, 60, 80, 100, and 120 | 40 |
| $f_{c,ic}$ (MPa) | 0, 20, 40, 60, 80, 100, and 120 | 40 |
| $f_{s,is}$ (MPa) | 200, 300, 400, 500, 600, and 700 | 200 |
| $f_{,os}$ (MPa) | 200, 300, 400, 500, 600, and 700 | 200 |
| $\bar{\lambda}$ | 0.2, 0.4, 0.6, 0.8, and 1.0 | 0.4 and 0.8 |
| $n$ | 0.1, 0.2, 0.3, 0.4, 0.5 and 0.55 | 0.4 |

discussed earlier, the rate of the increase is much higher for stocky columns than the slender columns. On the contrary, Fig. 13 (d) shows that increasing $t_o$ reduces the fire resistance time of the CFDST columns distinctly. This is because increasing $t_o$ results in the reduction of concrete area. As concrete carries more loads than steel tubes and offers higher fire resistance time than steel tubes, increasing $t_o$ results in a reduction in the fire resistance time.

The effects of the $D/B$ ratio on the fire resistance of CFDST columns are presented in Fig, 13 (c). The $D/B$ ratios were varied from 0.3 to 0.7 by keeping $B$ as well as the steel area fixed while changing $D$. The results show that the $D/B$ ratio has a greater effect on the fire behavior of slender columns compared to the stocky section. The critical time of the slender column increases by about 35 % as the $D/B$ ratio is increased. This is because the second moment of area of the internal steel tube is increased by raising the $D/B$ ratio, thereby enhancing the stiffness of the column under fire exposure, which coincides with the circular columns [24].

The $t_i/t_o$ ratio was determined by changing the $t_i$ and $t_o$ while keeping the $D$, $B$, and steel area constant. In general, Fig. 13 (f) illustrates that the $t_i/t_o$ ratio shows a limited impact on the fire performance. With the increase in the $t_i/t_o$ ratio, the fire resistance of the stocky column shows a slight increase, while for the slender columns, the change is very insignificant.

Fig. 13 (g) compares the fire resistance times of CFDST columns having square and circular shapes. The circular CFDST column has the same $D$, $t_i$, and steel area as the reference square CFDST column. As shown in Fig. 13 (g), under the same load ratio, a circular CFDST column has a longer fire resistance time than its square counterpart, particularly for the stocky column. However, for slender columns, the difference between their fire resistance times is small. For a square column, more areas are heated directly, meaning that the temperature within it rises faster. Consequently, the column reaches its fire resistance time earlier.

### 5.2. *Influences of material strength*

This section examines the effects of material strengths on the fire resistance of CFDST columns. As illustrated in Fig. 14 (a) and (b), increasing the strengths of the internal steel tube ($f_{s,is}$), and core concrete ($f_{c,ic}$) increases the fire resistance time of stocky columns; however, their impact on the fire response of slender columns is very minimal. This is because increasing the strength of materials can exert significant confining stresses on the core concrete, thereby enhancing the strength of the column exposed to fire. Accordingly, the fire resistance of the stocky column increases because its strength is governed by cross-sectional properties. For the slender column, however, its failure depends more on the column instability and second-order effect, leading to only a very slight increase in its fire resistance time when the $f_{s,is}$ and $f_{c,ic}$are increased.

The influences of external steel tube ($f_{s,os}$), and sandwiched concrete ($f_{c,oc}$) are shown in Fig. 14 (c). It can be observed from Fig. 14 (c) that generally increasing $f_{c,oc}$ results in an increase in the fire resistance significantly. The fire resistance time of the column is almost doubled as $f_{c,oc}$ increases from 20 to 120 MPa, regardless of the slenderness ratio. However, this conclusion is different from that obtained for circular CFSDT columns [24], namely, the fire resistance time is reduced by increasing the strength of the sandwiched concrete. This can be attributed to the different confining mechanisms at room temperature. Specifically, at room temperature, the external steel tube exerts confining stress on the sandwiched concrete, which depends on the material strength [52,53]. However, the confinement diminishes when the column is under fire exposure, weakening the bearing capacity of the column. Compared with the circular column, the confining stress provided by a square tube is lower. This means that the square column is less affected by the disappearing confinement, and its fire resistance rises with increasing $f_{c,oc}$ since the bearing capacity is enhanced by the high-strength concrete. Moreover, compared with the core concrete, the enhancement in the fire resistance due to the increase in the $f_{c,oc}$ is more significant. This is because the area of sandwiched concrete is larger than that of the core concrete, which impressively increases the stiffness of the column under fire exposure.

However, Fig. 14 (d) shows that, as the $f_{s,os}$ increases, the fire

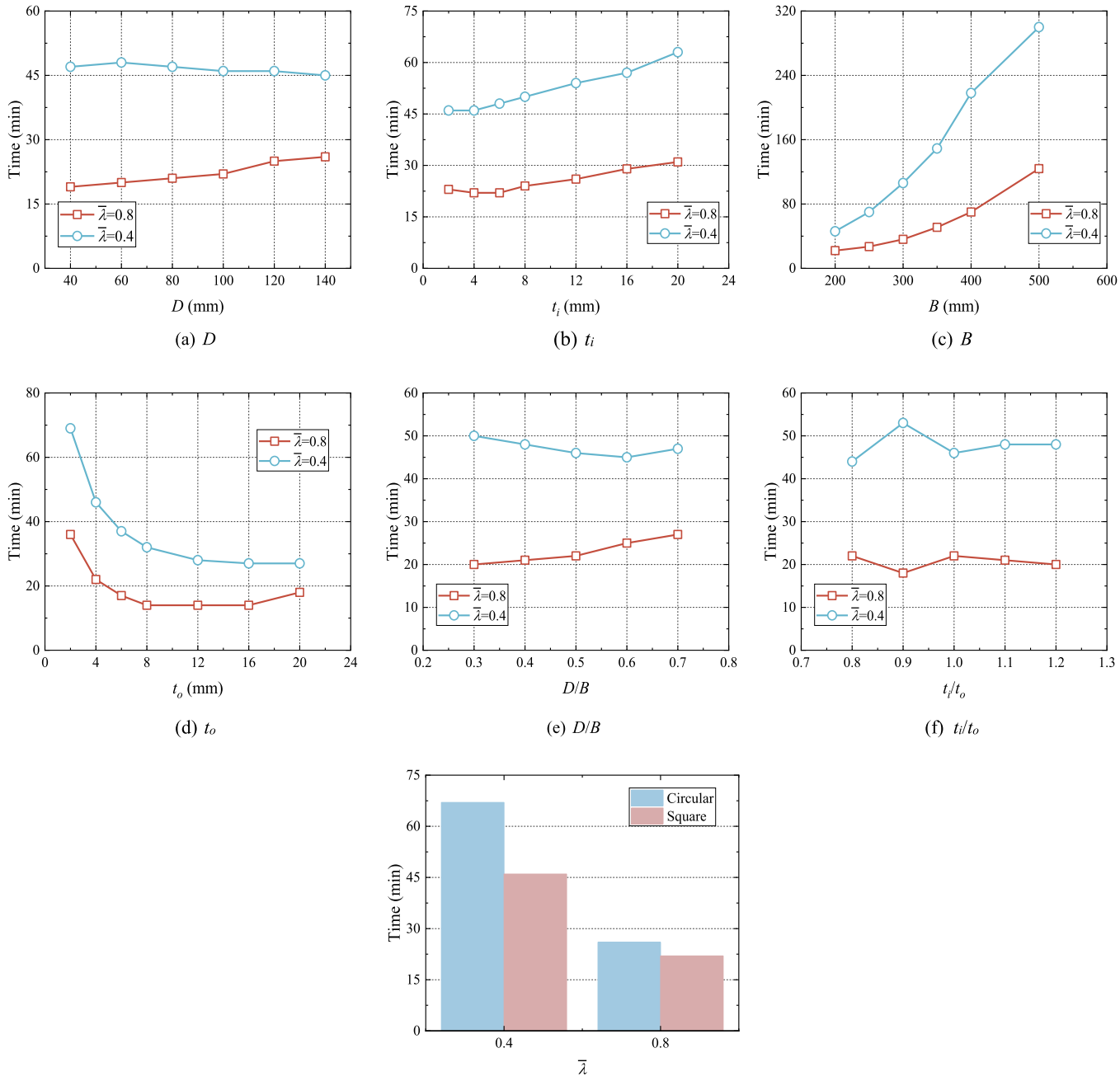


**Fig. 13.** Influences of cross-sectional properties on the fire resistance of CFDST columns.

resistance time of the columns decreases slightly for slender columns, but this reduction is significant for the stocky section. This is because the external tube is exposed to direct heating at the beginning, which decreases its fire resistance.

### 5.3. Influences of load ratio

The predicted fire resistance-load ratio curves for short and slender CFDST columns are given in Fig. 15. It is observed that increasing the load ratio ($n$) significantly decreases the fire resistance of CFDST columns. When $n$ increases from 0.1 to 0.55, the fire resistance time of the stocky and slender columns significantly reduces, and the decrements are similar, with values of 87 % and 91 %, respectively. Two reasons are responsible for this. First, with the increased load ratio, the second-order effects of the columns increase significantly, and a slender column is more likely to buckle. Second, as the load ratio increases, the material reaches its capacity earlier when it is under fire exposure, thereby shortening the fire resistance time of the column.

### 5.4. Influences of column slenderness ratio

As shown in Fig. 16, increasing the slenderness ratio ($\overline{\lambda}$) reduces the fire resistance time of CFDST columns significantly. When changing the slenderness ratio from 0.2 to$\overline{\lambda}$= 1.0, the fire resistance reduces by 65 % and 78 % for load ratios of 0.2 and 0.4, respectively. This outcome is predictable, as increasing the slenderness ratio decreases the ultimate load of the column due to second-order effects, making it more susceptible to buckling failure.

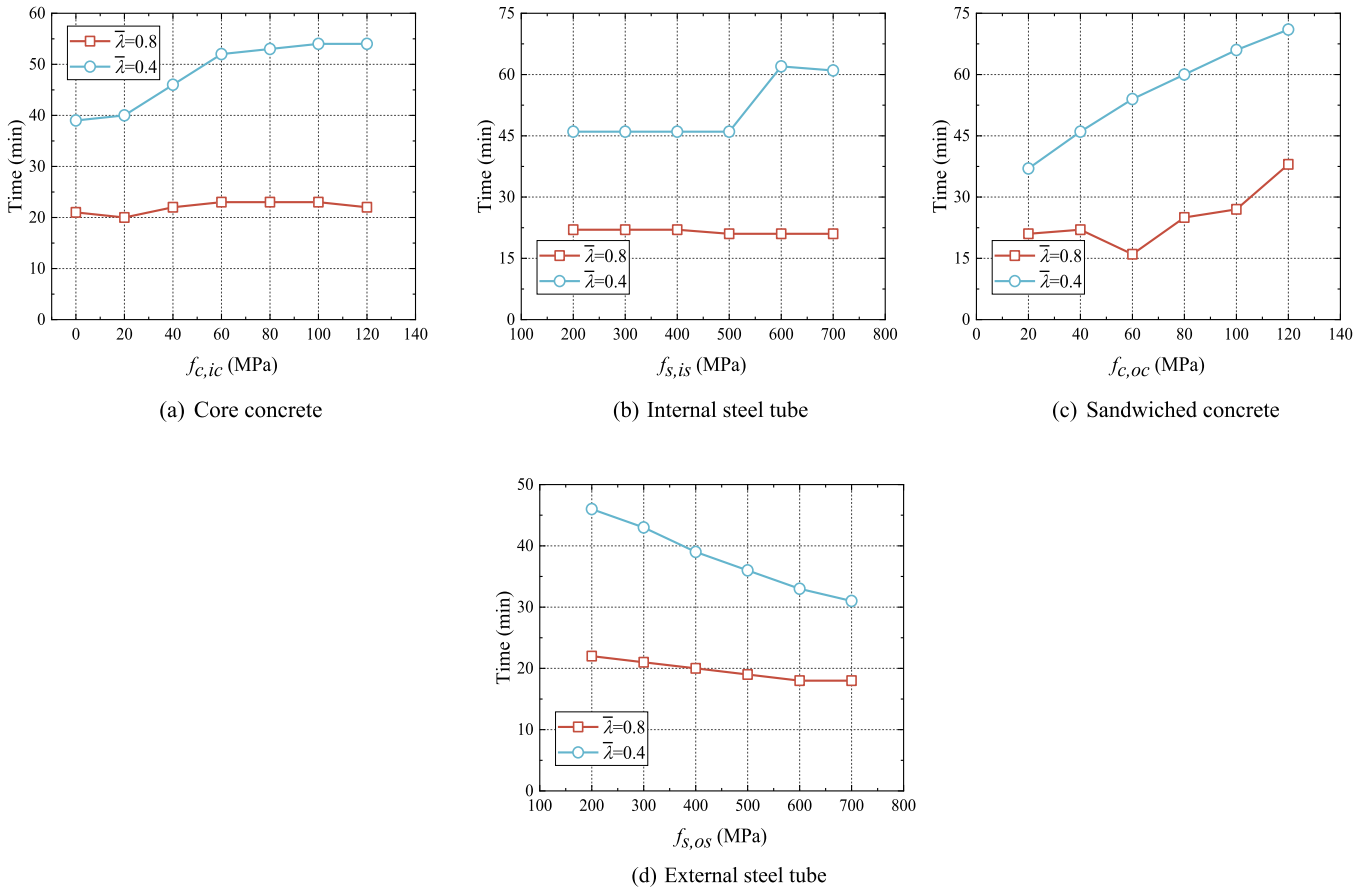


(a) Core concrete (b) Internal steel tube (c) Sandwiched concrete

(d) External steel tube

**Fig. 14.** Influences of material strengths of various components on the fire resistance of square CFDST columns.

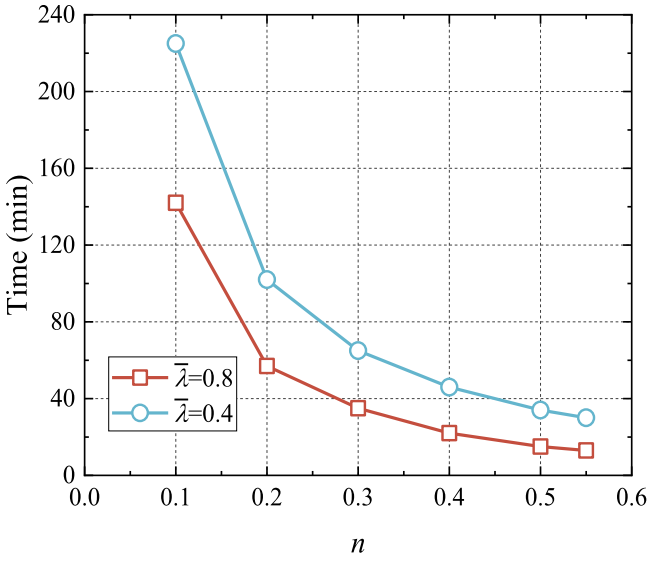


**Fig. 15.** Influences of load ratio on the fire resistance of CFDST columns.

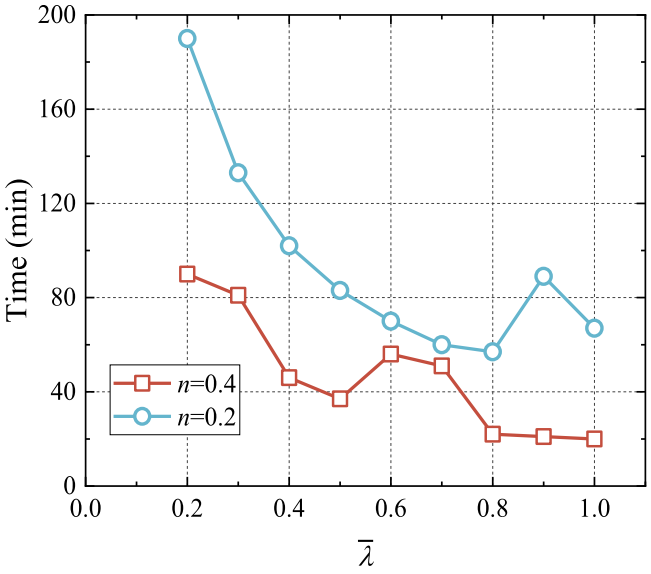


**Fig. 16.** Influences of slenderness ratio on the fire performance of CFDST columns.

## 6. Load distribution

This section discusses the load distribution of each component of both DSCFST and CFDST columns. The reference column is described in Section 5 and has a relative slenderness ratio of 0.2. The load sustained by each component was evaluated through normalized stress ($S_{33}/f_{20}$), where $S_{33}$ is the axial stress at z direction obtained from ABAQUS analysis and $f_{20}$ is the material strength at room temperature (20°).

Fig. 17 shows the load distribution in the DSCFST column. As illustrated earlier, the axial displacement curve can be divided into three parts. Initially, since the external tube is exposed to high temperatures directly, it expands thermally and becomes the main component sustaining the applied load. Consequently, the $S_{33}/f_{20}$ of the outer steel tube increases steadily while that of other components sees a stable decrease.

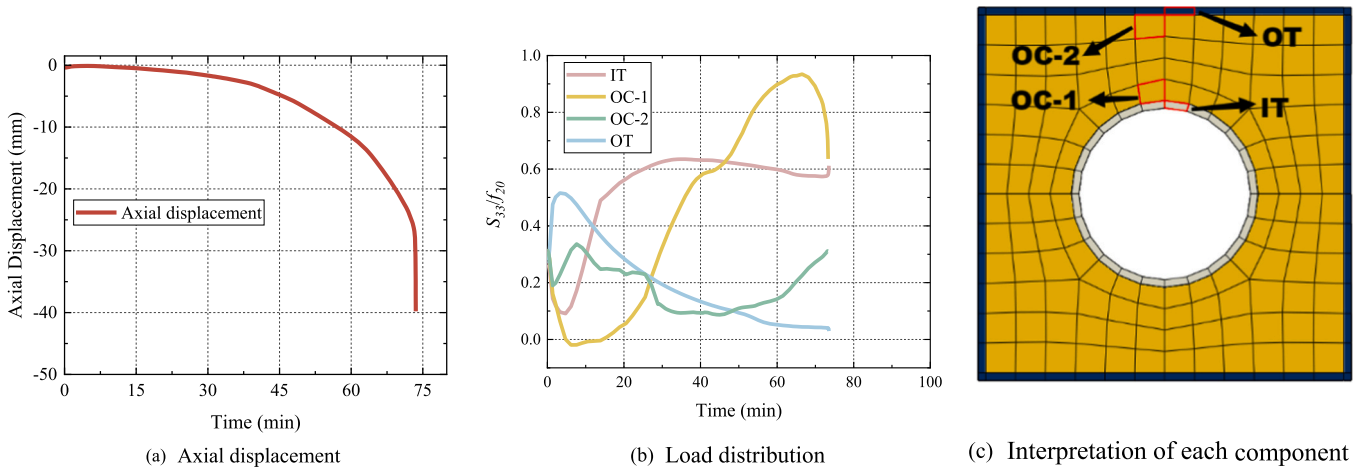


(a) Axial displacement (b) Load distribution (c) Interpretation of each component

**Fig. 17.** Load distribution of the square CFDST column.

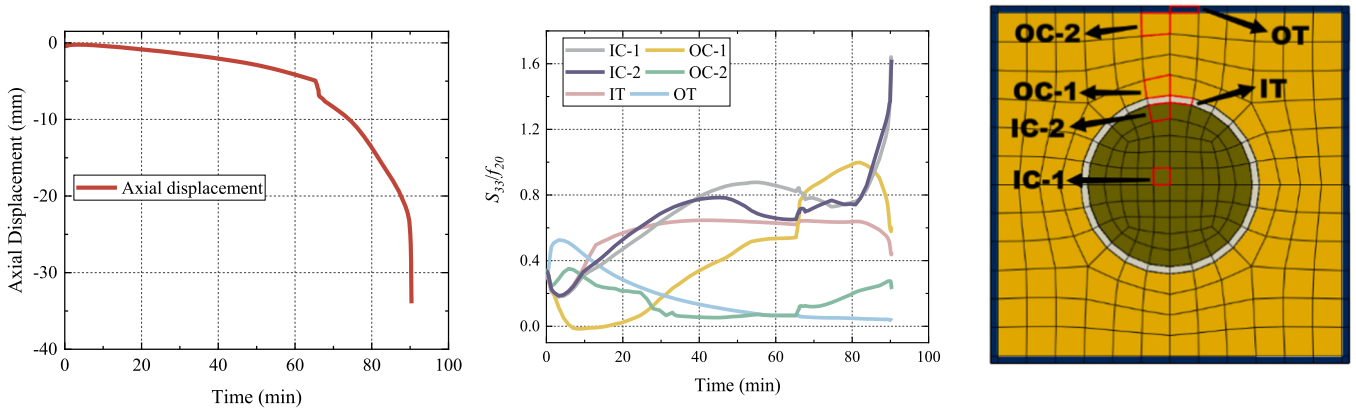


(a) Axial displacement (b) Load distribution (c) Interpretation of each component

**Fig. 18.** Load distribution of the square CFDST column.

During this stage, the axial displacement is almost unchanged. Next, the external steel tube yields, leading to a continuous decline in the $S_{33}/f_{20}$ of the external steel tube after reaching its peak at about 0.5. Meanwhile, the internal steel tube and concrete components gradually become the main components withstanding the applied load, being evidenced by a steady increase in their normalized stresses ($S_{33}/f_{20}$). After about 10 min of fire exposure, the $S_{33}/f_{20}$ of the sandwiched concrete (OC-1) decreases due to the material degradation, leading to a decline in the axial displacement. After 60 min, the normalized stress of the OC-1 decreases sharply, and the decline in the axial displacement accelerates. Eventually, axial displacement drops suddenly, indicating that the column has failed.

As shown in Fig. 18, the load distributions in sandwiched concrete and the steel tubes of the CFDST column resemble those of the DSCFST column when the fire exposure time does not exceed 60 min. When the outer steel tube yields, the normalized stress of the core concrete, the sandwiched concrete, and the internal steel tube increases significantly. This can be due to two reasons. Firstly, the ductility of the CFDST column is better than that of the DSCFST column. For instance, when the fire exposure time is 60 min, the axial displacements of the two types of columns are 10 mm and 5 mm, respectively. Secondly, the occasion in which the $S_{33}/f_{20}$ of the OC-1 starts to decrease is delayed compared to the DSCFST column, which means that the fire resistance of the CFDST column is enhanced significantly. Moreover, when the fire exposure time exceeds 80 min, the steel tubes and sandwiched concrete degrade, and their normalized stresses ($S_{33}/f_{20}$) drop significantly. In such a case, the core concrete is the main part sustaining the applied load, and its normalized stress ($S_{33}/f_{20}$) increases to a value higher than 1.0. However, since the cross-sectional area of the core concrete is limited, the axial displacement of the column shows an accelerating drop until failure. Hence, the above analysis indicates that the core concrete in CFDST columns delays the failure of the column by sustaining the applied load alone when other components are no longer able to carry the load.

## 7. Design method

There are no design models established for square CFDST columns exposed to fire. Zhu [24] proposed a fire design model for circular CFDST columns according to the design methods for reinforced CFST columns specified by EN 1994–1.2 [54] and Albero [55]. Similarly, in this study, the proposed model for CFDST columns exposed to fire treats the inner steel tube as the reinforced steel profile, and the predicted load ($N_{fi,Rd}$) is a function of a buckling factor ($\chi$) and plastic resistance at high temperatures ($N_{fi,pl,Rd}$), namely,

$$N_{fi,Rd} = \chi N_{fi,pl,Rd} \tag{5}$$

$$N_{fi,pl,Rd} = A_{is,\theta} f_{is,\theta} + A_{oc,\theta} f_{oc,\theta} + A_{os,\theta} f_{os,\theta} + \eta A_{ic,\theta} f_{ic,\theta} \tag{6}$$

$$\eta = \frac{0.5 k_e \xi_\theta}{1 + \xi_\theta} \tag{7}$$

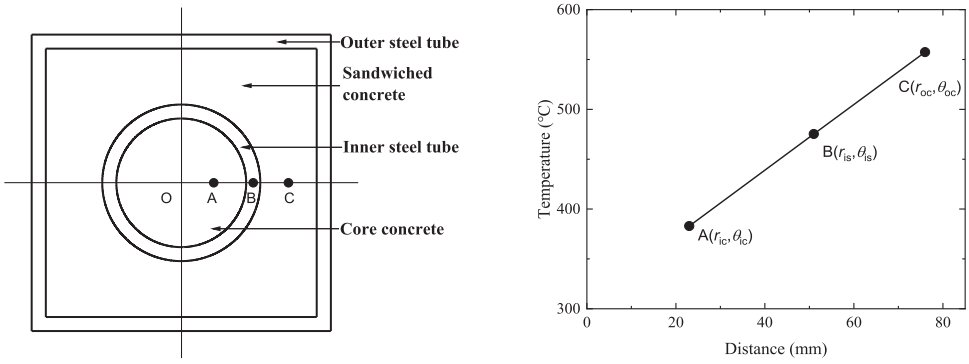


(a) Layers of a CFSDT column

(b) Linear interpolation of the equivalent temperature of the core concrete

**Fig. 19.** Determining the temperature of the core concrete.

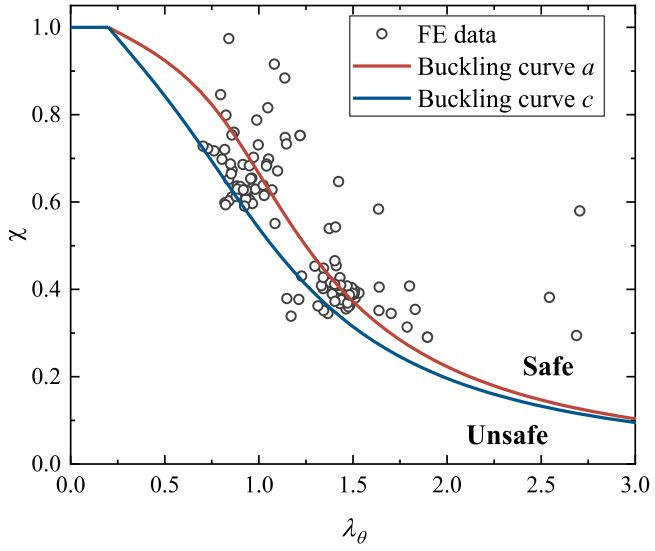


**Fig. 20.** Selection of the buckling curve.

$$\xi_\theta = \frac{A_{is,\theta} f_{is,\theta}}{A_{ic,\theta} f_{ic,\theta}} \tag{8}$$

in which $A_{i,\theta}$ is the area of steel and concrete, $f_{i,\theta}$ is the material strength at elevated temperatures, and $k_e$ equal to 1 for circular cross-section [56]. $\theta$ is the equivalent temperature for each component, of which the values of the steel tubes and sandwiched concrete are calculated according to Albero et al. [55]. In determining the equivalent temperature of the core concrete, as illustrated in Fig. 19, the concrete components and internal steel tube are divided into three layers, with A, B, and C denoting midpoints. Then, the temperature of the core concrete is calculated using a linear interpolation method as described by Eq. ( 9):

$$\theta_{ic} = \frac{\theta_{oc} - \theta_{is}}{r_{oc} - r_{is}} r_{ic} + \left(\theta_{oc} - \frac{\theta_{oc} - \theta_{is}}{r_{oc} - r_{is}} r_{oc}\right) \tag{9}$$

where $r_i$ is the distance between each midpoint to the center (point O). For instance, $r_{oc}$ indicates the distance between point C and point O.

The buckling factor ($\chi$) is defined in Clause 6.3.1.2 of EN 1993–1-1 [28] as:

$$\chi = \frac{1}{\Phi + \sqrt{\Phi^2 - \bar{\lambda}_\theta^2}} \tag{10}$$

$$\Phi = 0.5\left[1 + \alpha(\bar{\lambda}_\theta - 0.2) + \bar{\lambda}_\theta^2\right] \tag{11}$$

$$\bar{\lambda}_\theta = \sqrt{\frac{N_{fi,pl,Rd}}{N_{fi,cr}}} \tag{12}$$

$$N_{fi,cr} = \pi^2 (EI)_{fi,eff} \Big/ l_\theta^2 \tag{13}$$

$$(EI)_{fi,eff} = \varphi_{is,\theta} E_{is,\theta,\sigma} I_{is} + \varphi_{oc,\theta} E_{oc,\theta,\sigma} I_{oc} + \varphi_{os,\theta} E_{os,\theta,\sigma} I_s + \varphi_{ic,\theta} E_{ic,\theta,\sigma} I_{ic} \tag{14}$$

where $\alpha$ corresponds to the buckling curve. $\varphi_{i,\theta}$ is a reduction factor at elevated temperatures, and given by Albero et al. [55].

To check the accuracy of the design model, the selection of the buckling curve was verified first. In doing so, the FE results presented in Section 4 were used to calculate the buckling factor ($\chi$):

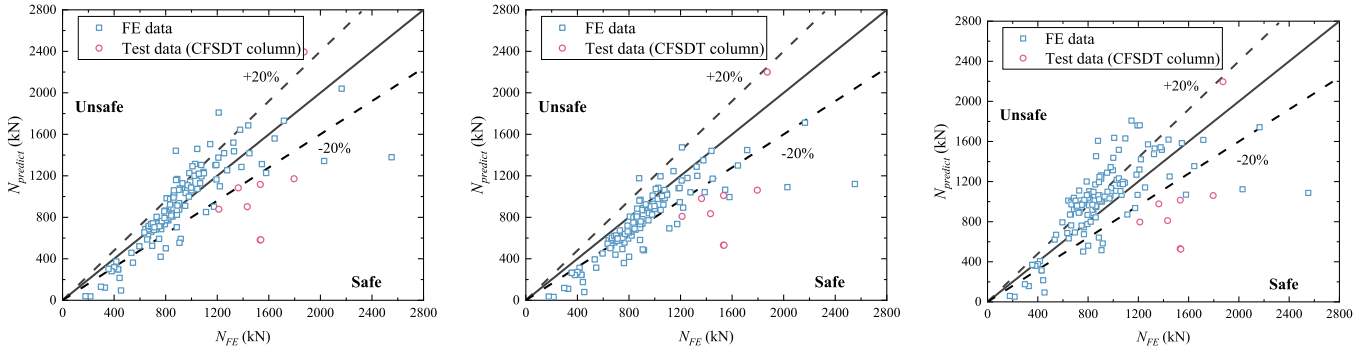


(a) Buckling curve "*a*"

(b) Buckling curve "*c*"

(c) EC4

**Fig. 21.** Validation of the predictions.

**Table 4**
Comparison of predicted and experimental loads of square CFDST columns.

| Column | $t$ (min) | $\bar{\lambda}_\theta$ | $N_{predict}$ (kN) | $N_r$ (kN) | $\xi$ | $\xi_{average}$ |
|---|---|---|---|---|---|---|
| F−1 | 92 | 0.39 | 836 | 1342 | −0.38 | −0.37 |
| F−2 | 111 | 0.40 | 834 | 1433 | −0.42 | |
| F−3 | 100 | 0.39 | 808 | 1212 | −0.33 | |
| F−4 | 98 | 0.44 | 980 | 1363 | −0.28 | |
| F−5 | 120 | 0.44 | 531 | 1533 | −0.65 | |
| F−6 | 131 | 0.46 | 530 | 1538 | −0.66 | |
| F−7 | 94 | 0.44 | 1061 | 1796 | −0.41 | |
| F−8 | 91 | 0.43 | 1009 | 1534 | −0.34 | |
| F−9 | 58 | 0.36 | 2199 | 1874 | 0.17 | |

$$\chi = \frac{N_{fi,Rd}^{FE}}{N_{fi,pl,Rd}} \tag{15}$$

in which $N_{fi,pl,Rd}$is derived from Eq. (6), and $N_{fi,Rd}^{FE}$ represents the load applied in the FE analysis. Fig. 20 illustrates the relationship between the buckling factor ($\chi$) and the relative slenderness ratio ($\bar{\lambda}_\theta$). Buckling curves "$a$" and "$c$" are compared for reference. The result illustrates that the buckling curve "$a$" may give unsafe predictions for square CFDST columns. The comparison of the predictions obtained by two buckling curves is shown in Fig. 21. In addition, the design method given in EN 1994–1-2, as used by Romero et al. [22] as well for circular CFDST columns, is also selected as a comparison. As can be seen from Fig. 21 the buckling curve "$c$" yields the safest predictions without losing accuracy, and only a few data points lay on the unsafe side. Accordingly, the buckling curve "$c$" is suggested for the design of square CFDST columns. Additionally, Table 4 illustrates the error ($\xi$) between the prediction ($P_{predict}$) and test data ($P_r$) of CFDST columns. The error ($\xi$) is calculated as ($P_{predict}/P_r - 1$), and a mean error of −0.37 is obtained which indicates that the model proposed in this study can estimate the performance of CFDST columns conservatively.

Nevertheless, consideration is required when applying the design model to real-world engineering practice. For instance, EN 1994 1.2 [57] states that when calculating the fire design load of a column in a frame, special consideration should be addressed in determining the buckling length of the column ($l_\theta$, see Eq. (13)), depending on the position of the column. This is because the performance of the column is affected by the structural continuity, and the column is axially and rotationally constrained by the adjacent members. This means that the boundary condition of the column may not be strictly pinned or fixed, which affects the calculation of the Euler buckling load. Hence, further studies should be conducted to investigate the effect of axial and rotational restraints on the design of the CFDST column under fire exposure.

## 8. Conclusions

This paper has presented the fire performance of square DSCFST and CFDST columns under concentric loads. A series of fire tests were undertaken, and FE models, along with the design model were developed and validated by the test observations. Based on the obtained results, the following conclusions can be drawn:

1. The CFDST columns having an inner steel tube filled with concrete have higher load-carrying capacity and ductility than DSCFST columns under fire exposure. In addition, the CFDST column with pinned-pinned end condition performs better in a fire than pinned-fixed end conditions.
2. Based on the test and FE analysis, the fire resistance of DSCFST columns is predominantly influenced by the load ratio and column slenderness ratio. As these ratios increase, there is a significant decrease in the fire resistance time of the columns. In addition, enhancing the fire performance of a slender square CFDST column can be achieved by increasing the thickness of the internal tube and by increasing the $D/B$ ratio.
3. Using thicker internal steel tubes or high-strength sandwiched concrete can increase the resistance of CFDST columns to fire. However, the use of high-strength or thick external steel tubes decreases the fire resistance.
4. The design model proposed yields accurate and safe fire resistance of square CFDST columns. The buckling curve "$c$" is suggested for the design of square CFDST columns exposed to fire.

## CRediT authorship contribution statement

**Xiao Kong:** Writing – original draft, Software. **Chenliu Li:** Writing – original draft, Software. **Qingtian Yang:** Writing – review & editing, Software. **Shicai Chen:** Writing – review & editing, Supervision, Project administration, Methodology, Funding acquisition, Conceptualization. **Qing Quan Liang:** Writing – review & editing, Supervision. **Habibah Ghazali:** Writing – review & editing, Visualization. **Mizan Ahmed:** Writing – original draft, Visualization, Supervision. **Hongjie Zhu:** Writing – original draft, Validation, Software, Methodology, Investigation, Formal analysis, Data curation, Conceptualization.

## Declaration of Competing Interest

The authors declare that they have no known competing financial interests or personal relationships that could have appeared to influence the work reported in this paper.

## Data Availability

Data will be made available on request.

## Acknowledgement

This support received from the National Natural Science Foundation of China (Grant No. 52278471) is acknowledged.

## References

[1] Uy B. Local and post-local buckling of concrete filled steel welded box columns. J Constr Steel Res 1998;47(1-2):47–72.
[2] Han L-H, Zhao X-L, Tao Z. Tests and mechanics model for concrete-filled SHS stub columns, columns and beam-columns. Steel Compos Struct 2001;1(1):51–74.
[3] Liang QQ, Uy B, Liew JYR. Local buckling of steel plates in concrete-filled thin-walled steel tubular beam–columns. J Constr Steel Res 2007;63(3):396–405.
[4] Huang Z, Li D, Uy B, Thai H-T, Hou C. Local and post-local buckling of fabricated high-strength steel and composite columns. J Constr Steel Res 2019;154:235–49.
[5] Ci J, Ahmed M, Tran V-L, Jia H, Chen S, Nguyen TN. Buckling resistance of axially loaded square concrete-filled double steel tubular columns. Steel Compos Struct 2022;43(6):689–706.
[6] Han LH, Tao Z, Huang H, Zhao XL. Concrete-filled double skin (SHS outer and CHS inner) steel tubular beam-columns. Thin-walled Struct 2004;42(9):1329–55.
[7] Tao Z, Han L-H. Behaviour of concrete-filled double skin rectangular steel tubular beam–columns. J Constr Steel Res 2006;62(7):631–46.
[8] Han J, Zuo J, Cheng WR. Experimental Study of Concrete-filled Double Steel Tubular Short Columns Subjected to Axial Compression Load. Earthq Resist Eng Retrofit 2008;30(1):28–35.
[9] Liew JYR, Xiong DX. Ultra-high strength concrete filled composite columns for multi-storey building construction. Adv Struct Eng 2012;15(9):1487–503.
[10] Ekmekyapar T, Al-Eliwi BJ. Concrete filled double circular steel tube (CFDCST) stub columns. Eng Struct 2017;135:68–80.
[11] Ahmed M, Liang QQ, Patel VI, Hadi MNS. Experimental and numerical studies of square concrete-filled double steel tubular short columns under eccentric loading. Eng Struct 2019;197:109419.
[12] Ahmed M, Liang QQ, Patel VI, Hadi MNS. Nonlinear analysis of square concrete-filled double steel tubular slender columns incorporating preload effects. Eng Struct 2020;207:110272.
[13] Ding F-X, Wang W-J, Lu D-R, Liu X-M. Study on the behavior of concrete-filled square double-skin steel tubular stub columns under axial loading. Structures 2020;23:665–76.
[14] Ci J, Ahmed M, Jia H, Chen S, Zhou D, Hou L. Experimental and numerical investigations of square concrete-filled double steel tubular stub columns. Adv Struct Eng 2021;24(11):2441–56.

[15] Chen S, Ahmed M, Ci J, Chen W, Sennah K. Behavior and design of axially loaded square concrete-filled double steel tubular slender columns. Adv Struct Eng 2022. 13694332221113041.
[16] Ma Q, Guo R, Zhao Z, Lin Z, He K. Mechanical properties of concrete at high temperature—A review. Constr Build Mater 2015;93:371–83.
[17] Tang Z, Zhang C. Effects of corrosion and pre-fatigue damage on the mechanical properties of HRB400E rebars. J Const Steel Res 2024;217:108641.
[18] Xiao J, Xie Q, Xie W. Study on high-performance concrete at high temperatures in China (2004–2016) - An updated overview. Fire Saf J 2018;95:11–24.
[19] Lu H, Han L-H, Zhao X-L. Fire performance of self-consolidating concrete filled double skin steel tubular columns: Experiments. Fire Saf J 2010;45(2):106–15.
[20] Liu X, Liu Z, Hui Y, Wang J. Research on the Concrete-Filled Double Skin steel Tubular (CFDST) columns subjected to axial force after fire. Structures, vol. 57. Elsevier,; 2023.
[21] Liu X, Liu Z, Mao X, Wang B, Fu H. Ultimate bearing capacity of concrete-filled double skin steel tubular (CFDST) columns under combined temperature and axial force. J Constr Steel Res 2024;219:108785.
[22] Romero ML, Espinos A, Portoles JM, Hospitaler A, Ibanez C. Slender double-tube ultra-high strength concrete-filled tubular columns under ambient temperature and fire. Eng Struct 2015;99:536–45.
[23] Camargo AL, Rodrigues JPC, Fakury RH, Laim L. Fire resistance of axially and rotationally restrained concrete-filled double-skin and double-tube hollow steel columns. J Struct Eng, ASCE 2019;145(11).
[24] Zhu H, Chen S, Ahmed M, Liang QQ. Experimental and numerical investigations of circular concrete filled steel double-skin and double-tube columns exposed to fire. Thin-Walled Struct 2024:111766.
[25] Lopes RF, Rodrigues JPC. Behaviour of restrained concrete filled square double-skin and double-tube hollow columns in case of fire. Eng Struct 2020;216:110736.
[26] Lopes RF, Rodrigues JPC, Correia AJP. Numerical modelling of composite steel and concrete double-skin and double-tube square cross-section columns subjected to fire. Fire Saf J 2023;139:103808.
[27] Abdelrahman A, Ghannam M, Lotfy S, AlHamaydeh M. Heat transfer in ultra-high-performance concrete-filled double-skin tubes under fire conditions. Fire Technol 2023;59(4):1519–54.
[28] Eurocode 3: Design of steel structures - Part 1–1: General rules and rules for buildings. European Committee for Standardization (CEN) Brussels, Belgium. 2005.
[29] GB/T 50081–2002: Standard for test method of mechanical properties on ordinary concrete. China Standard Press Beijing. 2003.
[30] GB/T 228.1-2010. Metallic Materials-Tensile Testing-Part 1: Method of Test at Room Temperature, Standardization Administration of the People's Republic of China 2010 China Standard Press Beijing,.
[31] ISO 834-1 Fire-resistance tests—elements of building construction—part 1: general requirements. Geneva (Switzerland 1999 International Standard Organization,.
[32] Liu J, Wei X, Yang Y, Yang W, Chen YF. Fire resistance of T-shaped concrete-filled steel tubular columns under eccentric compression. J Constr Steel Res 2021;187:106973.
[33] Wang JH, He J, Xiao Y. Fire behavior and performance of concrete-filled steel tubular columns: Review and discussion. J Constr Steel Res 2019;157:19–31.
[34] Guo Z, Wang X, Zhang XC, Song J, Li CF. Effects of boundary restraints on concrete-filled steel tubular columns with reinforcements exposed to fire. Thin-Walled Struct 2019;142:52–63.
[35] Jerath S. Structural stability theory and practice: buckling of columns, beams, plates, and shells. John Wiley & Sons,; 2020.
[36] Pires TA, Rodrigues JPC, Silva JJR. Fire resistance of concrete filled circular hollow columns with restrained thermal elongation. J Constr Steel Res 2012;77:82–94.
[37] Rodrigues JPC, Laím L. Fire resistance of restrained composite columns made of concrete filled hollow sections. J Constr Steel Res 2017;133:65–76.
[38] Espinos A, Romero ML, Hospitaler A. Advanced model for predicting the fire response of concrete filled tubular columns. J Constr Steel Res 2010;66(8-9):1030–46.
[39] Eurocode 1. Actions on structures–part 1–2: general actions–actions on structures exposed to fire. Brussels, Belgium: European Committee for Standardization (CEN),; 2002.
[40] Lie TT. Fire resistance of circular steel columns filled with bar-reinforced concrete. J Struct Eng, ASCE 1994;120(5):1489–509.
[41] Han L-H, Tan Q-H, Song T-Y. Fire performance of steel reinforced concrete columns. J Struct Eng 2015;141(4):04014128.
[42] Torelli G, Mandal P, Gillie M, Tran V-X. Concrete strains under transient thermal conditions: a state-of-the-art review. Eng Struct 2016;127:172–88.
[43] Torelli G, Gillie M, Mandal P, Tran V-X. A multiaxial load-induced thermal strain constitutive model for concrete. Int J Solids Struct 2017;108:115–25.
[44] Torelli G, Mandal P, Gillie M, Tran V-X. A confinement-dependent load-induced thermal strain constitutive model for concrete subjected to temperatures up to 500° C. Int J Mech Sci 2018;144:887–96.
[45] Wu JY, Chen WX, Zhou H. A length scale insensitive phase-field model for fully coupled thermo-mechanical fracture in concrete at high temperatures. Int J Numer Anal Methods Geomech 2022;46(14):2725–53.
[46] Pearce CJ, Nielsen CV, Bićanić N. Gradient enhanced thermo-mechanical damage model for concrete at high temperatures including transient thermal creep. Int J Numer Anal Methods Geomech 2004;28(7-8):715–35.
[47] Gernay T, Millard A, Franssen J-M. A multiaxial constitutive model for concrete in the fire situation: Theoretical formulation. Int J Solids Struct 2013;50(22-23):3659–73.
[48] A product of Dassault Systemes Simulia Corp Providence, RI, USA.
[49] Han L-H, Yang Y-F, Xu L. An experimental study and calculation on the fire resistance of concrete-filled SHS and RHS columns. J Constr Steel Res 2003;59(4):427–52.
[50] CEN E. Hot finished structural hollow sections of non-alloy and fine grain steels. Part 2: Toler, Dimens Sect Prop 2006.
[51] Ahmed M, Liang QQ, Patel VI, Hadi MNS. Local-global interaction buckling of square high strength concrete-filled double steel tubular slender beam-columns. Thin-Walled Struct 2019;143:106244.
[52] Ahmed M, Liang QQ, Patel VI, Hadi MN. Numerical analysis of axially loaded circular high strength concrete-filled double steel tubular short columns. Thin-Walled Struct 2019;138:105–16.
[53] Ci JC, Jia H, Ahmed M, Chen SC, Zhou DX, Hou LQ. Experimental and numerical analysis of circular concrete-filled double steel tubular stub columns with inner square hollow section. Eng Struct 2021;227.
[54] EN-1992-1-2 Eurocode 2: Design of concrete structures - part 1-2: General rules - Structural fire desiggn 2004 European Committee for Standardization (CEN), Brussels, Belgium.
[55] Albero V, Espinos A, Romero ML, Hospitaler A, Bihina G, Renaud C. Proposal of a new method in EN1994-1-2 for the fire design of concrete-filled steel tubular columns. Eng Struct 2016;128:237–55.
[56] Yu M, Zha X, Ye J, Li Y. A unified formulation for circle and polygon concrete-filled steel tube columns under axial compression. Eng Struct 2013;49:1–10.
[57] EN and Standard E. Eurocode 4: Design of composite steel and concrete structures - Part 1–2: General rules - Structural fire design. 2004;